

THE EQUATION OF STATE FROM LATTICE QCD*

EDWIN LAERMANN

Fakultät Physik, Universität Bielefeld
Universitätsstrasse 25, 33615 Bielefeld, Germany*(Received January 27, 2010)*

Numerical results on the QCD equation-of-state from lattices with temporal extents 4, 6 and 8 are presented. The computations have been performed within two different discretization schemes, the p4 and the asqtad actions which improve lattice artefacts for thermodynamic observables at high temperatures. In the course of these computations also observables that are sensitive to deconfinement and chiral symmetry restoration were analyzed. In addition, quantities measuring fluctuations and correlations of baryon number, strangeness and electric charge have been studied.

PACS numbers: 11.15.Ha, 11.10.Wx, 12.38.Gc, 12.38.Mh

1. Introduction

The equation of state (EoS) of hot and strongly interacting matter is a fundamental property of finite temperature QCD, not only from a theoretical point of view but also phenomenologically. For instance, the interpretation of experimental results from heavy ion colliders relies on the determination of energy density and pressure as well as on an understanding of deconfinement and chiral symmetry.

Under RHIC and LHC conditions the net baryon density of hot matter created in these experiments is small so that for most questions lattice results obtained at vanishing chemical potentials are appropriate. In this region the transition from the low temperature hadronic to the high temperature plasma regime most likely is continuous and fluctuations are not expected to show singular behavior. Nevertheless, fluctuations and their higher moments even if computed at vanishing chemical potential not only give insight into the relevant degrees of freedom at a given temperature but also hint towards nearby singularities either in the chiral limit or at a possible critical point in the QCD phase diagram [1].

* Talk presented at the EMMI Workshop and XXVI Max Born Symposium "Three Days of Strong Interactions", Wrocław, Poland, July 9–11, 2009.

In the present contribution our results on the equation of state, *i.e.* pressure, energy and entropy density are summarized. Furthermore, deconfinement and chiral symmetry restoration as well as fluctuations and correlations of certain quantum numbers are discussed. Due to steady technical progress the necessary lattice computations can now be performed with a quark mass spectrum which is (almost) realistic. It is, however, important to control discretization effects. Therefore, the results presented here have been generated on the basis of so-called improved actions which were designed to reduce the effects of non-vanishing lattice spacing (a) at high temperature. Moreover, the calculations were carried out at different values of a . An extensive discussion of the discretization effects, however, is beyond the scope of this contribution and I refer to [2–5] in this regard.

2. The equation of state

2.1. Computational setup

The results for the equation-of-state presented here are for (2+1)-flavor QCD. They have been obtained from lattices with temporal extent $N_\tau = 4, 6$ and 8, corresponding to different lattice spacings $aT = 1/N_\tau$, and are based on high statistics numerical simulations performed with two different improved discretization schemes for staggered fermions, the tadpole improved asqtad action [6] and the tree level improved p4 action [7]. For details of the generation of the gauge field configurations we refer to [2–4].

For each finite temperature calculation that entered the analysis of the equation of state, a corresponding “zero temperature” calculation has been performed at the same value of the gauge coupling and for the same set of bare quark mass values, in order to determine the necessary UV normalizations. Moreover, “zero temperature runs” were needed to fine-tune the bare lattice parameters as follows. Apart from the lattice size, $N_\sigma^3 \times N_\tau$, the partition function, as well as any lattice observable, depends on the lattice spacing a , the bare gauge coupling, $\beta = 6/g^2$, and the bare light and strange quark masses, $\hat{m}_u = \hat{m}_d = \hat{m}_l$ and \hat{m}_s , respectively. The bare quark masses have been tuned at $T = 0$ such as to correspond to fixed Goldstone¹ mass m_π and fixed kaon mass m_K in physical units. This defines a so-called “line of constant physics”. It turned out that fixing the light to strange quark mass ratio to $m_l/m_s = 1/10$ leads to a constant ratio between m_π and m_K of $m_\pi/m_K = 0.435(2)$ (p4) and $0.437(3)$ (asqtad). Tuning \hat{m}_s such that the kaon adopts its physical value then leads to a Goldstone mass of about

¹ In the staggered fermion formulation only one of the light quark pseudo-scalar states has a mass vanishing in the chiral limit. The other states have masses of $\mathcal{O}(a^2)$ which vanish only in the continuum limit.

220 MeV for the p4 action². In these fine-tunings the parameters r_n that characterize the shape of the static quark potential,

$$\left(r^2 \frac{dV_{\bar{q}q}(r)}{dr} \right)_{r=r_0} = 1.65, \quad \left(r^2 \frac{dV_{\bar{q}q}(r)}{dr} \right)_{r=r_1} = 1.0, \quad (1)$$

were used as physical scales³. The ratio r_0/r_1 has been determined in the two discretization schemes consistently, $r_0/r_1 = 1.4636(60)$ (p4 [3]) and $1.474(7)(18)$ (asqtad [8]). Finally, to determine the scales r_0 and r_1 and the temperature in physical units (MeV) we have related them to properties of the bottomonium spectrum and use the value $r_0 = 0.469(7)$ fm determined from the $\mathcal{T}(2S - 1S)$ splitting in calculations with the asqtad action [9].

2.2. The trace anomaly

The starting point for the computation of pressure and energy density is the trace anomaly

$$\frac{\Theta_\mu^\mu}{T^4} = \frac{\varepsilon - 3p}{T^4} = T \frac{\partial}{\partial T} (p/T^4), \quad (2)$$

where it is understood that UV divergences are removed by subtracting the corresponding zero temperature value. On our line of constant physics the trace anomaly is obtained as the expectation value

$$\frac{\Theta_\mu^\mu(T)}{T^4} = -R_\beta(\beta) N_\tau^4 \left(\left\langle \frac{d\bar{S}}{d\beta} \right\rangle_T - \left\langle \frac{d\bar{S}}{d\beta} \right\rangle_{T=0} \right), \quad (3)$$

where \bar{S} denotes the average action and $R_\beta = T d\beta/dT = -ad\beta/da$ is the β function. Like the action, Θ can be separated into a gluonic (Θ_G) and a fermionic (Θ_F) part, with $\Delta\langle \dots \rangle = \langle \dots \rangle_{T=0} - \langle \dots \rangle_T$,

$$\begin{aligned} \frac{\Theta_G^{\mu\mu}(T)}{T^4} &= R_\beta N_\tau^4 \Delta\langle \bar{S}_G \rangle \\ \frac{\Theta_F^{\mu\mu}(T)}{T^4} &= -R_\beta R_m N_\tau^4 \left\{ 2\hat{m}_l \Delta\langle \bar{\psi}\psi \rangle_l + \hat{m}_s \Delta\langle \bar{\psi}\psi \rangle_s \right\}, \end{aligned} \quad (4)$$

where S_G is the gluon action and $\langle \bar{\psi}\psi \rangle_{l,s}$ denote the chiral condensates. R_m is the mass renormalization function $\hat{m}(\beta)R_m(\beta) = d\hat{m}(\beta)/d\beta$. This form

² The fine-tunings for the two actions have been carried out by different groups independently and prior to the collaborative effort reported on here, with the result that the strange mass is slightly larger for the asqtad action [4].

³ Note that for the comparison of results obtained with different actions, an accurate value of r_n in physical units (1/MeV) is not necessary as only $r_n T$ is needed.

for the trace anomaly holds for fixed m_l/m_s ratio and for the p4 action; because of tadpole improvement the formulae for the asqtad action are slightly more complicated, see [4]. The β function R_β has been calculated non-perturbatively from the numerical data on $\hat{r}_n = r_n/a$ as $R_\beta/\hat{r}_n = d\beta/d\hat{r}_n$. For that purpose, \hat{r}_n was parametrized by the perturbative two-loop β function modified by a rational function. In the same way, R_m was determined from the fine-tuned $\hat{m}(\beta)$ values. Together with high statistics data on the gluon action and the chiral condensate differences, the results for the trace anomaly depicted in Fig. 1 were derived.

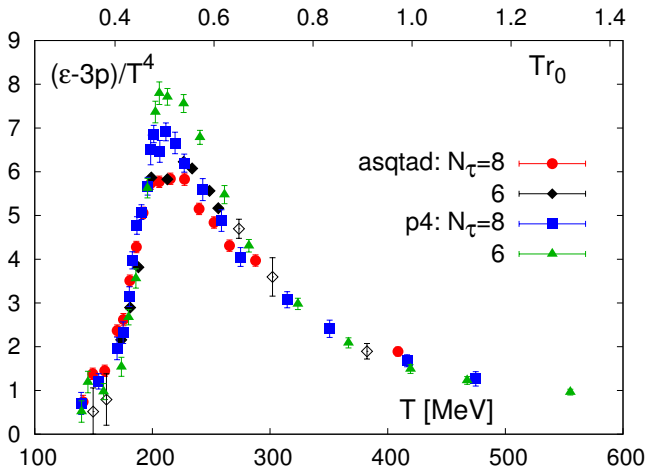


Fig. 1. The trace anomaly $(\epsilon - 3p)/T^4$ calculated on lattices with $N_\tau = 6$ and 8. Here and in the following figures, the upper x -axis shows the temperature in units of r_0 , Eq. (1), while the lower x -axis gives the temperature in units of MeV.

The figure highlights very consistent results between the two discretization schemes. The biggest discretization effects occur in the intermediate temperature regime. These differences are mainly caused by the fermionic contribution to Θ_μ^μ , which accounts for less than 15% of the total value, and can be traced back to the large nonperturbative contributions to R_m at low β values [4].

The results for the low as well as the high temperature regime are shown in more detail in Fig. 2. At low T the differences between $N_\tau = 6$ and 8 are mainly due to a shift of the crossover temperature of about 5–7 MeV. For comparison the figure also includes the predictions of the hadron resonance gas (HRG) model [10] which has been quite successful in characterizing the particle abundancies observed in heavy ion collisions. It remains to be seen whether the observed discrepancies to the HRG are due to residual quark mass and discretization effects or whether they hint at a genuine difference.

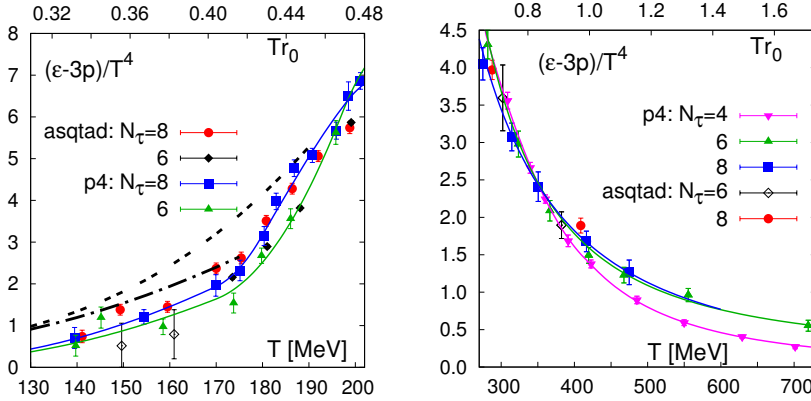


Fig. 2. The trace anomaly at low (left) and high temperatures (right). At low T , solid lines show interpolation curves for the p4 action. The other curves give the trace anomaly calculated in a hadron resonance gas model with two different cuts for the maximal mass, $m_{\max} = 1.5 \text{ GeV}$ (dashed-dotted) and 2.5 GeV (dashed). At high T , the curves show fits to the data based on Eq. (5).

At high temperature $(\varepsilon - 3p)/T^4$ drops quickly and eventually approaches zero $\sim g^4(T) \sim 1/\ln^2(T/\Lambda)$. However, in the investigated temperature range we observe a stronger decay of the trace anomaly. We, therefore, fit the data by

$$\left(\frac{\varepsilon - 3p}{T^4}\right)_{\text{high-}T} = \frac{3}{4}b_0g^4 + \frac{d_2}{T^2} + \frac{d_4}{T^4}, \quad (5)$$

where the first term gives the leading order perturbative result and the other terms parametrize nonperturbative corrections as inverse powers of T^2 . While the temperatures reached are not large enough to identify the logarithmic T dependence, the fit without the perturbative contribution describes the data very well.

2.3. Pressure, energy and entropy

The pressure is obtained from the trace anomaly by integrating Eq. (2) over temperature,

$$\frac{p(T)}{T^4} - \frac{p(T_0)}{T_0^4} = \int_{T_0}^T dT' \frac{1}{T'^5} \Theta^{\mu\mu}(T'). \quad (6)$$

Here T_0 is an arbitrary temperature value in the low temperature regime which has been chosen as $T_0 = 0$ where $p = 0$. As an estimate of the systematic effects we also used $T_0 = 100 \text{ MeV}$ and the HRG pressure value

at this temperature as the starting point for the integration. The difference is shown as the black box in Fig. 3 (left). With pressure and $\varepsilon - 3p$ at hand one can compute energy (ε) and entropy density ($s = (\varepsilon + p)/T$) which are also shown in Fig. 3. Both quantities show a rapid increase in a small temperature range and approach the Stefan–Boltzmann limit from below rather slowly. Based on the small differences between the two actions and the different N_τ values we conclude [4] that this behavior is describing the EoS at high temperatures very well, with deviations from the continuum limit of at most 5% at $T \geq 200$ MeV.

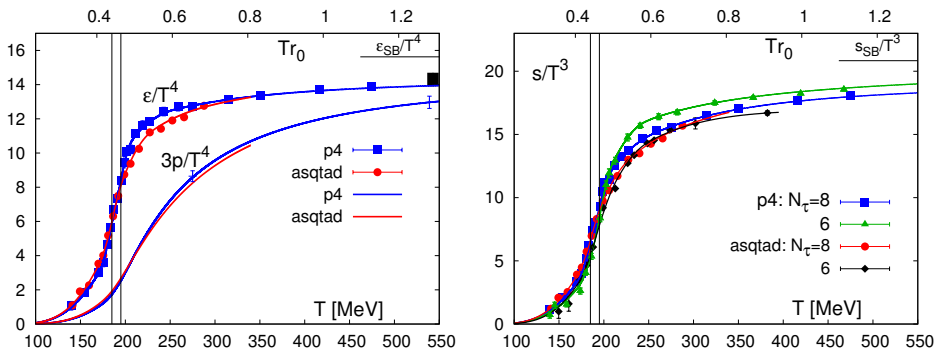


Fig. 3. Energy density and three times the pressure (left) and the entropy density (right). The black bar at high temperature in the left plot indicates the systematic shift of data that would arise from matching to a hadron resonance gas at $T = 100$ MeV. The bands indicate the temperature region $185 \text{ MeV} < T < 195 \text{ MeV}$.

2.4. Deconfinement and chiral symmetry

The rapid rise of the energy and entropy density in a narrow temperature interval is already reflecting the release of many new degrees of freedom, *i.e.* deconfinement. The genuine order parameter for this transition is the Polyakov loop but strictly so only for infinitely heavy quarks. In the presence of quarks with finite mass the Polyakov loop ceases to be an order parameter in the sense of detecting the spontaneous breakdown of a global symmetry, here the center symmetry of the gauge group. Still, it is related to the free energy $F_{Q\bar{Q}}(R)$ of a static $Q\bar{Q}$ pair at distance R ,

$$L_{\text{ren}}(T) = \exp(-F_{Q\bar{Q}}(R \rightarrow \infty, T)/2T) \quad (7)$$

after multiplicative renormalization [11]. As Fig. 4 (left) shows, also at small quark masses the Polyakov loop exhibits a marked rise in the same T interval where we observe changes in the EoS.

The transition to the quark–gluon plasma is expected to also restore chiral symmetry. In the chiral limit a genuine order parameter for this transition is the chiral condensate, vanishing in the phase of chiral symmetry restoration. Away from the chiral limit, chiral symmetry is explicitly broken by the nonvanishing quark mass. Additionally, the condensate receives an additive contribution which diverges quadratically in the continuum limit and is proportional to the quark mass. In order to remove this UV divergence we use the subtracted condensate [3]

$$\Delta_{l,s}(T) = \frac{\langle \bar{\psi}\psi \rangle_{l,T} - \frac{m_l}{m_s} \langle \bar{\psi}\psi \rangle_{s,T}}{\langle \bar{\psi}\psi \rangle_{l,0} - \frac{m_l}{m_s} \langle \bar{\psi}\psi \rangle_{s,0}}, \tag{8}$$

where the denominator at $T = 0$ cancels the multiplicative renormalization factor. This quantity is shown in Fig. 4 (right) where the $N_\tau = 6$ data have been shifted by 7 and 5 MeV, respectively to account for a shift in the crossover temperature. As the figure shows, the chiral condensate drops in the same temperature region where the Polyakov loop as well as *e.g.* the energy density rise. The data thus indicate that an approximate restoration of chiral symmetry takes place in the same temperature interval as deconfinement.

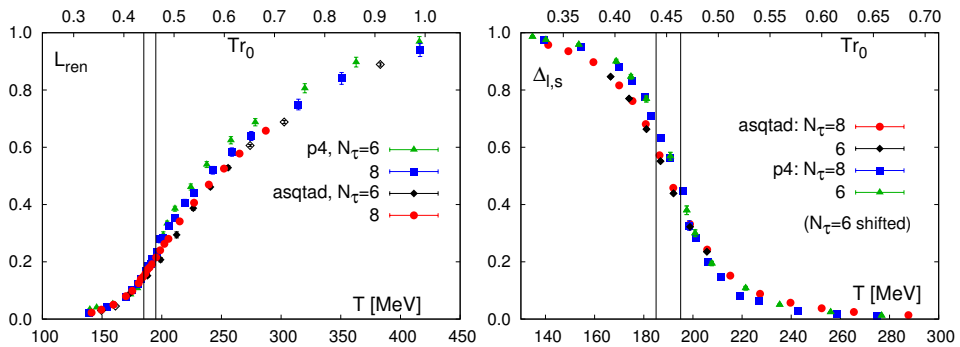


Fig. 4. Left: The renormalized Polyakov loop. Right: The subtracted chiral condensate normalized to the corresponding $T = 0$ values. The data for $N_\tau = 6$ have been shifted by -7 MeV (asqtad) and -5 MeV (p4).

3. Fluctuations and correlations

At non-vanishing chemical potentials $\mu_{u,d,s}$ for u , d and s quarks, the pressure can be obtained from a Taylor expansion [12] in the potentials,

$$\frac{p}{T^4} = \sum_{i,j,k} c_{ijk}(T) \left(\frac{\mu_u}{T}\right)^i \left(\frac{\mu_d}{T}\right)^j \left(\frac{\mu_s}{T}\right)^k. \tag{9}$$

While this approach allows to address the EoS at least at small values for the potentials, the Taylor coefficients also give access to fluctuations and correlations of certain quantum numbers at $\mu_i = 0$. These quantities probe deconfinement aspects of the QCD transition and are related to event-by-event fluctuations in heavy ion collisions [13, 14].

In Fig. 5 we show the results for the light and strange quark number susceptibilities, $\chi_l = 2c_{200}$ and $\chi_s = 2c_{002}$, respectively, where the u and d quark potentials have been set equal throughout this paper. The data exhibit a rapid rise in the same temperature interval where also energy density, chiral condensate and Polyakov loop show drastic changes. The quadratic light quark fluctuations, χ_l , rapidly approach the Stefan–Boltzmann limit while this approach is slower for the heavier strange quarks. Note that at low temperature χ_s receives contributions only from the lightest strange particles and therefore is not sensitive to the singular behavior of the partition function in the chiral limit.

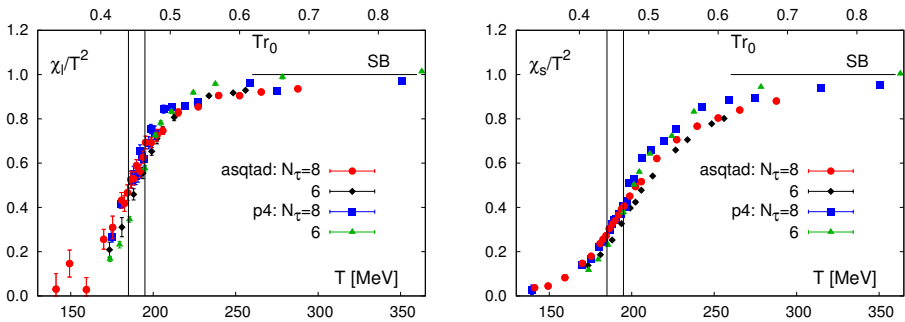


Fig. 5. The quadratic fluctuations χ_i for light (left) and strange (right) quark number on $N_\tau = 6$ and 8 lattices for the asqtad and the p4 fermion action.

The coefficients c_{ijk} of the expansion (9) in the quark chemical potentials are related [5] to the coefficients χ_{ijk}^{BQS} of a similar expansion in the potentials for baryon number B , strangeness S and electric charge Q . The ratios of quartic and quadratic fluctuations of B and S are shown in Fig. 6 and compared with the results from the HRG and the Stefan–Boltzmann values. We plot ratios because in the HRG they are much less sensitive to details of the hadron spectrum. In fact, in the Boltzmann approximation to the HRG model, *i.e.* considering all baryons as heavy on the temperature scale, χ_4^B / χ_2^B is independent of the hadron masses and equals 1. This is reasonably well reproduced by the lattice data at low temperature. Note however the rise of the ratio in the vicinity of the transition which is expected to become more pronounced in the chiral limit. Even within the Boltzmann approximation the structure of the HRG is more complicated in the strange (and charged)

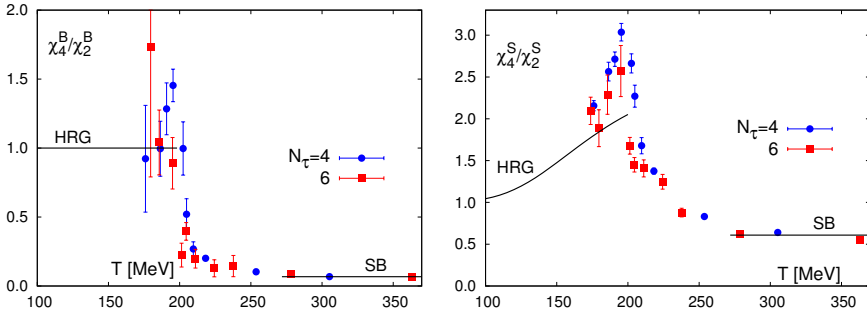


Fig. 6. The ratios of fourth and second order cumulants for baryon number (left) and strangeness (right) obtained on $N_\tau = 4$ and 6 lattices with the p4 action. The curves depict the HRG predictions.

sector. In these cases multiply strange (or charged) hadrons contribute and enhance the quartic fluctuations. This qualitative feature is also indicated by the data.

At temperatures above $1.5 T_c$ the analysis of the fluctuations, *i.e.* their rapid approach to the Stefan–Boltzmann values already suggests light and strange quarks as the carriers of conserved quantum numbers. As a further test one may study correlations between the different charges [14, 15]. Results for correlations of B with Q and S are shown in Fig. 7. Here, at low temperature only strange or electrically charged hadrons contribute to the numerators. Hence, the ratio χ_{11}^{BQ} approaches $1/2$ at $T = 0$ because neutrons are not electrically charged. Similarly, χ_{11}^{BS} becomes zero in the same limit as the lightest baryons do not carry strangeness. In the high temperature limit we have two quarks with electric charge $-1/3$ and one with $+2/3$ thus giving zero in the BQ and 1 in the BS correlation. These values are indeed rapidly approached by the data above the transition temperature.

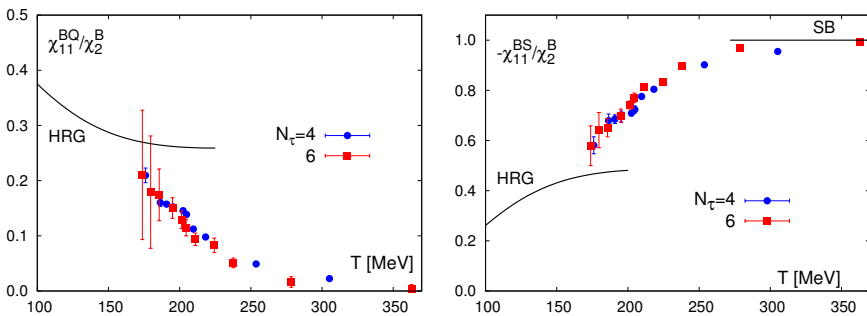


Fig. 7. Correlations of baryon number with electric charge (left) and strangeness (right). The data have been normalized to the quadratic fluctuations of baryon number and are compared to predictions of the HRG.

In summary, we conclude that already at rather low temperatures of about 1.5 times the transition temperature fluctuations and correlations of conserved charges are well described by an ideal massless quark gas. In the hadronic regime the HRG provides a qualitative description of the data. However, there are indications from higher moments that the HRG fails in the vicinity of the transition.

While the presented analyses have been carried out with light quarks that are one tenth of the strange quark mass, calculations with physical light quark masses and smaller lattice spacings are needed to gain deeper insight into the range of applicability of the HRG at low temperatures and into nonperturbative features of QCD in the transition region. For the latter, it will also be interesting to lower the light quark masses beyond their physical values to eventually study critical behavior [16] in the approach to the chiral limit.

I wish to thank the organizers for the kind invitation to an interesting and charming XXVI Max-Born symposium.

REFERENCES

- [1] For reviews see *e.g.* M. Stephanov, *Acta Phys. Pol. B* **35**, 2939 (2004); V. Koch, [arXiv:0810.2520](#).
- [2] C. Bernard *et al.*, *Phys. Rev.* **D75**, 094505 (2007).
- [3] M. Cheng *et al.*, *Phys. Rev.* **D77**, 014511 (2008).
- [4] A. Bazavov *et al.*, *Phys. Rev.* **D80**, 014504 (2009).
- [5] M. Cheng *et al.*, *Phys. Rev.* **D79**, 074505 (2009).
- [6] K. Orginos, D. Toussaint, *Phys. Rev.* **D59**, 014501 (1999); K. Orginos, D. Toussaint, R.L. Sugar, *Phys. Rev.* **D60**, 054503 (1999).
- [7] U. M. Heller, F. Karsch, B. Sturm, *Phys. Rev.* **D60**, 114502 (1999).
- [8] C. Aubin *et al.*, *Phys. Rev.* **D70**, 094505 (2004).
- [9] M. Wingate *et al.*, *Phys. Rev. Lett.* **92**, 162001 (2004); A. Gray *et al.*, *Phys. Rev.* **D72**, 094507 (2005).
- [10] J. Cleymans, K. Redlich, *Phys. Rev.* **C60**, 054908 (1999); A. Andronic, P. Braun-Munzinger, J. Stachel, *Nucl. Phys.* **A772**, 167 (2006).
- [11] O. Kaczmarek *et al.*, *Phys. Lett.* **B543**, 41 (2002).
- [12] C.R. Allton *et al.*, *Phys. Rev.* **D66**, 074507 (2002); R. Gavai, S. Gupta, *Phys. Rev.* **D68**, 034506 (2003).
- [13] S. Jeon, V. Koch, *Phys. Rev. Lett.* **85**, 2076 (2000).
- [14] V. Koch, A. Majumdar, J. Randrup, *Phys. Rev. Lett.* **95**, 182301 (2005).
- [15] R. Gavai, S. Gupta, *Phys. Rev.* **D73**, 014004 (2006).
- [16] S. Ejiri *et al.*, *Phys. Rev.* **D80**, 094505 (2009) [[arXiv:0909.5122\[hep-lat\]](#)].